

Division - Soil Use and Management | Commission - Soil and Water Management and Conservation

# Soil loss as a desertification risk indicator: mapping and simulation in the Salitre River Sub-Basin, Northeast Brazil

Márcio Lima Rios<sup>(1)\*</sup> , Alisson Jadavi Pereira da Silva<sup>(2)</sup>  and Vagson Luiz Carvalho-Santos<sup>(3)</sup> 

<sup>(1)</sup> Universidade Federal de Minas Gerais, Instituto de Geociências, Programa de Pós-Graduação em Geografia, Belo Horizonte, Minas Gerais, Brasil.

<sup>(2)</sup> Instituto Federal de Educação, Ciência e Tecnologia Baiano, Governador Mangabeira, Bahia, Brasil.

<sup>(3)</sup> Universidade Federal de Viçosa, Departamento de Física, Viçosa, Minas Gerais, Brasil.

**ABSTRACT:** Discussions on desertification frequently highlight soil erosion as a striking feature of this phenomenon. In particular, the high spatial density of gullies represents a strong indication of the formation of desertification hotspots. In this study, through field activities and Monte Carlo simulations, we estimated the volume of soil loss by linear erosion on the slopes of the middle course of the Salitre river in the North of Bahia State. This estimative contributes to the recognition of a desertification process in the studied local. The lengths of the gullies and rills, visible through high-spatial-resolution satellite images, were vectorized. The width and depth of the Linear Erosion Features (LEFs) were measured through field study and recorded via geoprocessing. Statistical treatment was applied to the data to indicate the probability of occurrence of the width and depth classes. Subsequently, the Monte Carlo simulation was used to indicate the volume of soil removed from the slopes by the linear erosion process. Several ramified systems of LEFs are identified and mapped. Monte Carlo simulation fits the measured data well. Estimates indicate that linear erosion event eroded approximately 450,000 m<sup>3</sup> of soil in an area of 2,000 hectares, which indicates extreme land degradation.

**Keywords:** soil erosion, geoprocessing, Monte Carlo method, Gullies.

\* **Corresponding author:**

E-mail: marciogeog@gmail.com

**Received:** November 07, 2019

**Approved:** January 23, 2020

**How to cite:** Rios ML, Silva AJP, Carvalho-Santos VL. Soil loss as a desertification risk indicator: mapping and simulation Salitre River Sub-Basin, Northeast Brazil. Rev Bras Cienc Solo. 2020;44:e0190159.

<https://doi.org/10.36783/18069657rbcs20190159>

**Copyright:** This is an open-access article distributed under the terms of the Creative Commons Attribution License, which permits unrestricted use, distribution, and reproduction in any medium, provided that the original author and source are credited.



## INTRODUCTION

Despite being hugely controversial, discussions about the desertification problem focus on environmental degradation in areas that are vulnerable and pressed by anthropic action. The United Nations Convention to Combat Desertification (UNCCD) defines the desertification phenomenon as the degradation of the lands in arid, semiarid, and dry sub-humid areas, resulting from various factors, including natural causes and human activities, mainly associated with the inadequate use of soils, water, and vegetation (United Nations, 1994). Desertification is associated mainly with the degradation of soil, vegetation, and changes in climate and hydrological conditions (D'Odorico et al., 2013). These aspects yield significant changes in ecosystems, impacting in the biodiversity and socio-economic activities. Several studies performed in different parts around the world, like Italy (Salvati et al., 2016), Greece (Karamesouti et al., 2018), China (Huang and Siegert, 2006), Irã (Sarparast et al., 2018), Mexico (Becerril-Piña et al., 2015), Africa (Capozzi et al., 2018), and Brazilian Northeast (Vieira et al., 2015), show that the desertification process can be caused by anthropogenic exploitation on the natural resources.

The desertification process produces effects on regional and global scales. For instance, in a regional scale, the soil degradation in a river basin will alter the essential components of the hydrological cycle, such as water infiltration and storage in the soil, runoff, and evapotranspiration. On the other hand, a non-local consequence of desertification is the production and transport of dust to other regions, inducing a large-scale effect (Johnson et al., 2011; Middleton, 2017, 2018). Finally, the deteriorating livelihoods resulting from diminishing crop productivity, recurrent climatic extremes, and political instability may result in large-scale human migrations, with significant environmental, socio-economic, and political consequences (Myers, 1993; Bates, 2002; Lu et al., 2016).

The discussions on desertification frequently highlight soil degradation as a marked characteristic of the process (Valentin et al., 2005). Soil erosion and sedimentation have been proposed as valuable indicators of desertification (Wasson et al., 2002; Krause et al., 2003; Dawelbait and Morari, 2011). Soils support (directly or indirectly) most forms of life on Earth, and the loss of soil resources, which is accelerated by the development of agriculture and livestock grazing, has historically threatened food security and induced the collapse of some societies (Diamond, 2005).

The generation of desertification indicators for a region demands the conduction of studies on soil erosion, especially on linear erosion in the form of rills and gullies. The existence of rills on a slope indicates a more advanced stage of erosion because the formation of channels implies that a large amount of soil has been removed (Bigarella, 2003; Descroix et al., 2008). Bigarella (2003) states that rills constitute ephemeral and discontinuous features. Nevertheless, the concentrated runoff normally deepens the rills, causing the collapse of the interior walls of the incision, and the headwaters advance upstream, removing many particles, and dragging them downstream. This fact means that the formation of rills is promptly followed by its evolution, and consequent increment in soil losses (Poesen et al., 2003; Chaplot et al., 2005).

Gullies are relatively permanent features on the slopes (more extended and more profound than rills) and are associated with the processes of accelerated erosion, and consequently, with the instability of the landscape (Poesen et al., 2003). The gully formation is a consequence of both the natural landscape evolution and the impact of anthropic action. Indeed, gullies represent signs of instability on a slope, caused by alterations in the environment, and humans are just one of the agents of these changes. Nevertheless, the formation of gullies is accelerated when there are quick changes in the landscape caused by human action (Chaplot et al., 2005). Additionally, it is a broad and advanced stage of land degradation and slope dissection, represented by the downstream

movement of sediments, which causes an imbalance in the quality of soils, local biota, and fluvial channels.

On a river basin and/or sub-basin level, the description of the quantity, shape, and length of the existing rills and gullies require exhaustive measurements performed at the site. This is a complex task that involves uncertainties generated by the variability in the shape of the transverse sections of the rills and gullies (Casalí et al., 2015). The set of values of the cross-section shapes of the existing rills and gullies in an area will hardly follow a normal distribution, making the use of average and mean values inadequate to estimate the eroded soil volume. One alternative to attenuate these problems is the use of satellite images (Dawelbait and Morari, 2011) integrated with non-parametric statistical methods such as the Monte Carlo method (Gimenez et al., 2004; Sidorchuk, 2005; Huang and Siegert, 2006; Lal et al., 2015; Cuomo et al., 2016). Mathematical simulation, in combination with cartographic studies, is becoming one of the main approaches for the quantitative description of degradation processes in agro landscapes (Kulik et al., 2013).

Based on the above, this work aimed to identify LEFs and estimating the volume of soil loss due to linear erosion occurring on the slopes near the middle course of the Salitre river. This estimative allowed us to recognize that there is a desertification process under development at this hydrographic sub-basin of the semiarid of Bahia, Brazil. Indeed, this work contributes to reinforcing the findings of Santos (2016), which has recognized this area under the action of an accelerated desertification process. Our results determine one of the most critical indicators of desertification, the linear soil erosion (Avni, 2005).

Although several studies discuss the desertification associated with the erosive phenomenon (Avni, 2005; Salvati et al., 2015; Dai et al., 2017; Sarparast et al., 2018; Zweig et al., 2018), desertification processes occurring in the Brazilian Northeast are poorly studied. Therefore, the mapping of LEFs and the estimation of soil loss are crucial to be used as an indicator of desertification processes. In this context, from obtained data in field activities, we propose to use the Monte Carlo method to estimate the volume of soil loss from the formation of ravines and gullies. Monte Carlo calculations consist of an exciting tool for this issue because its randomness allows inserting uncertainty in the evaluated parameters. Therefore, the main novelty of the proposed methodology is that the estimation of soil loss in a vast region having soil with the same physical properties can be estimated from obtaining geometrical data of a fraction of the observed ravines and gullies.

## MATERIALS AND METHODS

### Studied area

The experimental region is located in a rural area of Campo Formoso municipality, state of Bahia-Brazil, along the middle course of the Salitre River sub-basin (Figure 1), close to the bed of the main river (between the coordinates: 10° 10' 25" S, 40° 44' 55" W and 40° 45' 16" W, 10° 19' 28" S), corresponding to a narrow deep valley depression. The Salitre River emerges in the Northern portion of Chapada Diamantina and ends in the São Francisco River (Governo do Estado da Bahia, 2017).

The central part of the sub-basin of the Salitre river is characterized by a planed surface, established on a carbonate plateau (Brito Neves et al., 2012), where the watercourses are well carved and with narrow floodplains (Silva, 2006). The geological materials are mainly carbonated rocks of the Caatinga Formation, with calcrete lithologies (Brito Neves et al., 2012; Borges et al., 2016), covered by soils susceptible to erosion, mainly Haplic Cambisols and Litholic Neosols (*Cambissolo Háplico Ta Eutrófico* and *Neossolo Litólico Eutrófico*) (Naime et al., 2007).

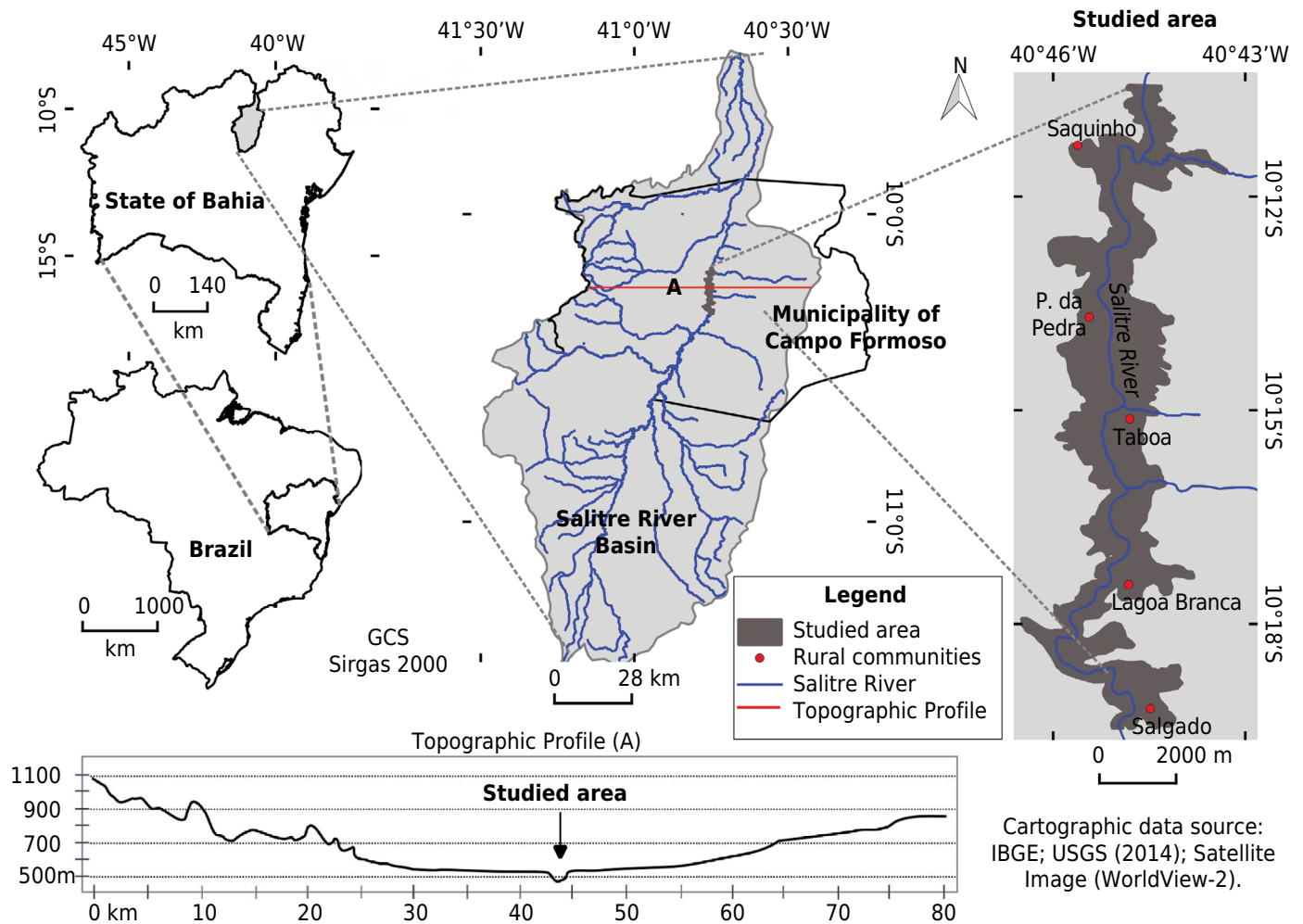


**Figure 1.** Location map of the studied area.

The studied area consists of a narrow valley bottom depression following the Salitre River (Figure 1), from South to North, along the carbonate plateau. Within this depression, there are steeper slopes, above 10 %, and embedded drainage, with an altimetric variation of approximately 60 m, between the edge of the plateau and the Salitre river bed (USGS, 2014). The delimited space consists of a polygon, which was able to include the morphologically lowered area and with a significant presence of LEFs. Besides, according to Carlini (2013) and Santos (2016), this region presents a low density of vegetation cover and extensive patches with exposed soils.

Additionally, the region has a semiarid climate with a mean annual temperature above 25 °C and rainfall ranging from 400 to 500 mm yr<sup>-1</sup>, concentrated between November and March (Governo do Estado da Bahia, 2017). The potential evapotranspiration at Salitre Weather Station (9° 30' S, 40° 38' W) is around 1,900 mm yr<sup>-1</sup> (Embrapa, 2019). The aridity indices (ratio between precipitation and potential evapotranspiration) of middle course locations of the Salitre are between 0.25 and 0.36 (Santos, 2016). The aridity index below 0.5 demonstrates reduction and high evapotranspiration, being widely used as one of the desertification risk indicators (Spinoni et al., 2015).

### Mapping of linear erosion features using high-resolution satellite images

The area was visualized using the program Google Earth, which allowed obtaining previous plan-altimetric information, to determine the sites and collect topographic data at the field. Through a navigation GPS, a travel itinerary was developed such that we could

transversely cross the Salitre River (East-West/West-East) by constructing transects in three different portions of the area (South, Central, and North), aiming at understanding the topographical context of the area (Figure 2).

The mapping of the LEFs and the delimitation of the degraded area was performed using high-resolution orthorectified images from the satellite WorldView-2. The images had a resolution of 0.5 cm and were dated May 15, 2015. We then proceeded with the digitization (linear vector) of the LEFs visualized in the image, using the program Quantum GIS 2.8. The adopted methodology is based on the visual interpretation of the primary elements (location, tone/color) and secondary elements (size, shape, and texture). Rills and gullies were identified from the continuous lines highlighted on the image, especially by the differences in coloration, tonality, texture, and shape. Small and discontinuous erosion channels along the slope were not considered due to the limit of the spatial resolution of the images. The data on location, quantity, and length of the erosion lines were directly extracted through the QGIS, and it served as the basis for the calculations soil losses caused by the linear erosion process on the slopes.

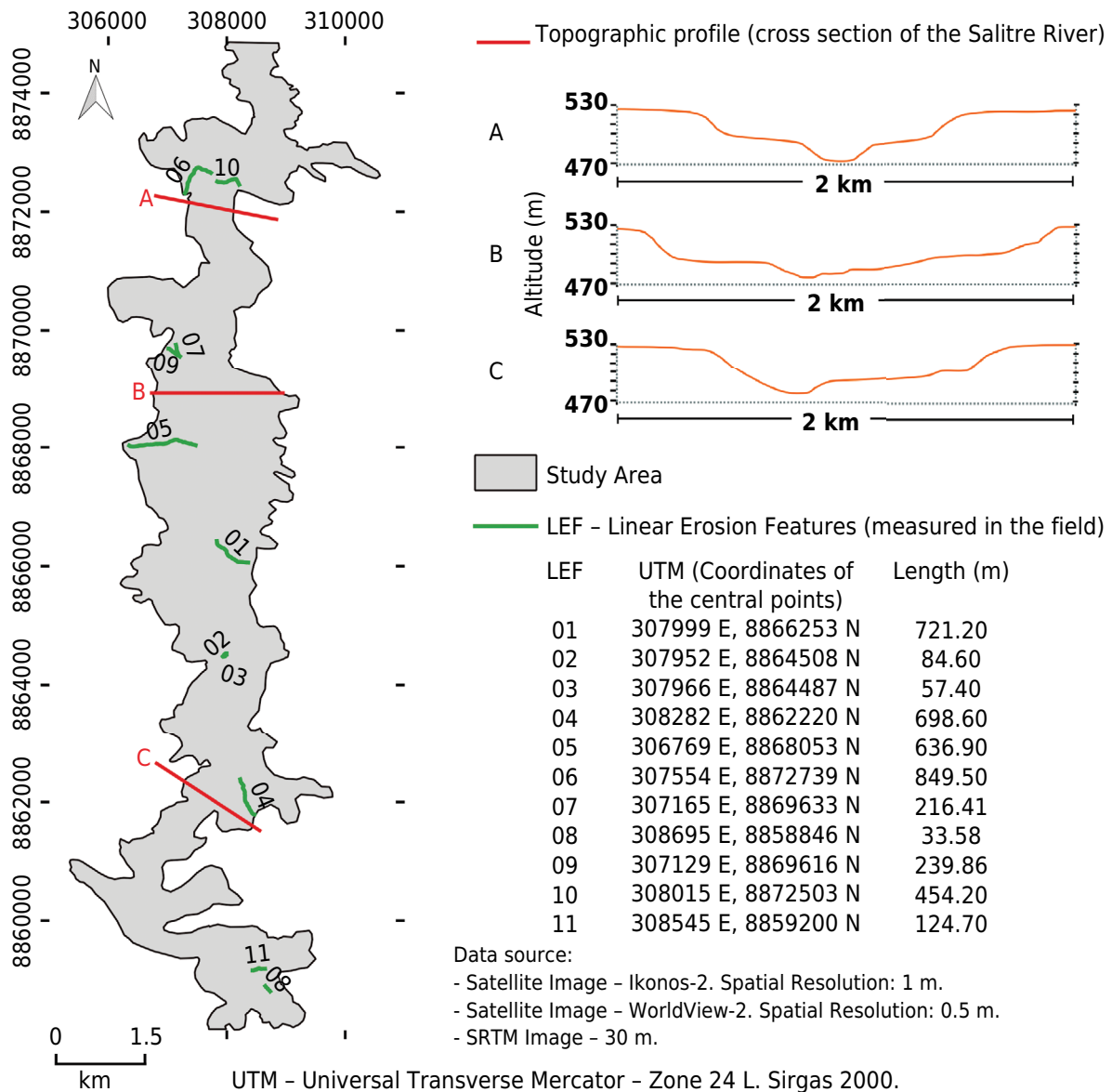


**Figure 2.** The map presents the spatial distribution of LEFs (linear erosion features) obtained from the field measurements and show the topographic profiles (cross-section of the Salitre River) in the studied area.

The next step was the random selection of 11 LEFs (distributed in the area) for field measurement of width, depth, and shape variables. The selected LEFs are shown in figure 2, in which we also present the length and location of each LEF measured.

### Soil loss estimation

Aiming to determine the eroded soil volume, the values of length of the rills and gullies identified in the area were obtained via satellite images. At the site, the following variables we have obtained some experimental data to characterize LEFs (based on cross-sections) for soil loss estimation: (i) width of extreme points of the LEFs (WE); (ii) width inside the LEFs (WI); (iii) depth of WE (DE); (iv) depth of WI (DI); and (v) shape (Figure 3). The performed measurements were performed in intervals of 15 m along the lines of 11 LEFs, randomly sampled to ensure proper statistical distribution of the above-described quantities. Each site of measurement of the variables formed a sampling point, which was georeferenced. The width and depth were measured along a section transverse to the length of the incision in the soil. Visual interpretation and photographic records were used to determine whether the walls of the incisions were U-shaped (walls close to 90°) or V-shaped (inclined walls). Figure 3 illustrates the measurement of the variables in the sampling sites.

The variables were measured from a total of 201 cross-sections (sampling). The obtained data were subjected to the Kolmogorov-Smirnov test to verify the hypothesis of normal distribution. After confirming the hypothesis of non-normality of the obtained values of WE, WI, DE, and DI, Monte Carlo simulations (Rubinstein and Kroese, 2007; Landau and Binder, 2014) were performed to simulate the occurrence of all the variables in the entire extension of the linear features existing in the area. From the 201 cross sections sampled, a total of 9,701 sections were simulated for the whole studied area.

The Monte Carlo method was developed as follows: initially, the total length of the gullies/rills and the distance between the cross-sections of data collection were inserted, and, after that, the averaged value of each frequency range for the variables WE, WI, DE, and DI were given as initial data. With this data, the program performs four random selections of a number between 0 and 1. The random number is divided into 13 ranges, following the percentages of occurrence obtained during the field activities. The first, second, third, and fourth selections determine the probability of the gully section presents WE, WI, DE, and DI respectively. A fifth number is randomly selected to determine whether the simulated cross-section corresponds to a U- or V-shaped rill/gully, using the frequency measured for these two shapes. To have more confidence in the simulated data, this

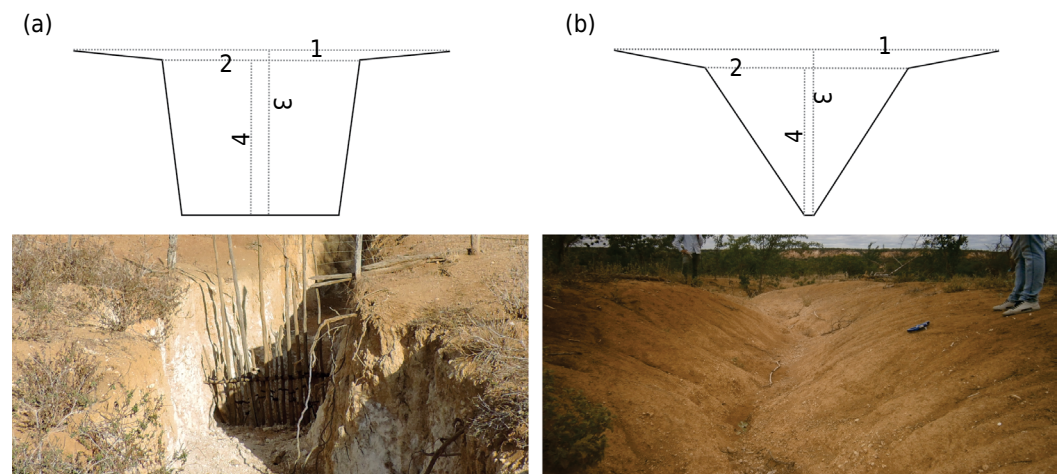


**Figure 3.** Illustrations and photographs of the typologies of shapes of the linear erosion features (LEFs). U-shaped linear incision (a); V-shaped linear incision (b). 1: width of extreme points of the LEFs (WE); 2: width inside the LEF (WI); 3: depth from WE (DE); 4: depth from WI (DI).

procedure was repeated using 20 different seeds for generating the random numbers, until all cross-sections of the studied area have been simulated.

After obtaining all the values of WE, WI, DE, and DI, the geometry of two consecutive cross-sections of the gullies were approximated using two overlapped trapezoidal solids (Figure 4). The volume of this geometrical structure is given by equation 1.

$$\text{Vol} = \frac{L}{3} [(A_{MS} + A_{ms} + \sqrt{A_{MS}A_{ms}}) + (A_{MI} + A_{mi} + \sqrt{A_{MI}A_{mi}})] \quad \text{Eq. 1}$$

in which  $L$  is the distance between two measured cross-sections,  $A_M$  and  $A_m$  are, respectively, the areas of the trapezia at the extremities  $M$  and  $m$  of the trapezoidal solid. The sub-indices  $S$  and  $I$  indicate the upper and lower trapezia, respectively. The upper trapezium is considered as the one formed by a geometrical structure whose sides are given by WE, WI, and (DE-DI). The lower one will be the trapezium with sides WI, B, and DI, where  $B = \min(\text{WI}-10 \text{ cm}, 15 \text{ cm})$  depends on the shape of the erosion feature. In other words, if it is U-shaped, the side WI-10 cm is considered; if it is V-shaped, the shortest side of the trapezium will be equal to 15 cm. After calculating the geometrical parameters and volumes from the 20 different seeds, we have averaged the 20 obtained values aiming at having more confident values.

The verification of Monte Carlo simulation was done using the standard Nash-Sutcliffe Efficiency (NSE) statistics (Nash and Sutcliffe, 1970), as recommended by Moriasi et al.

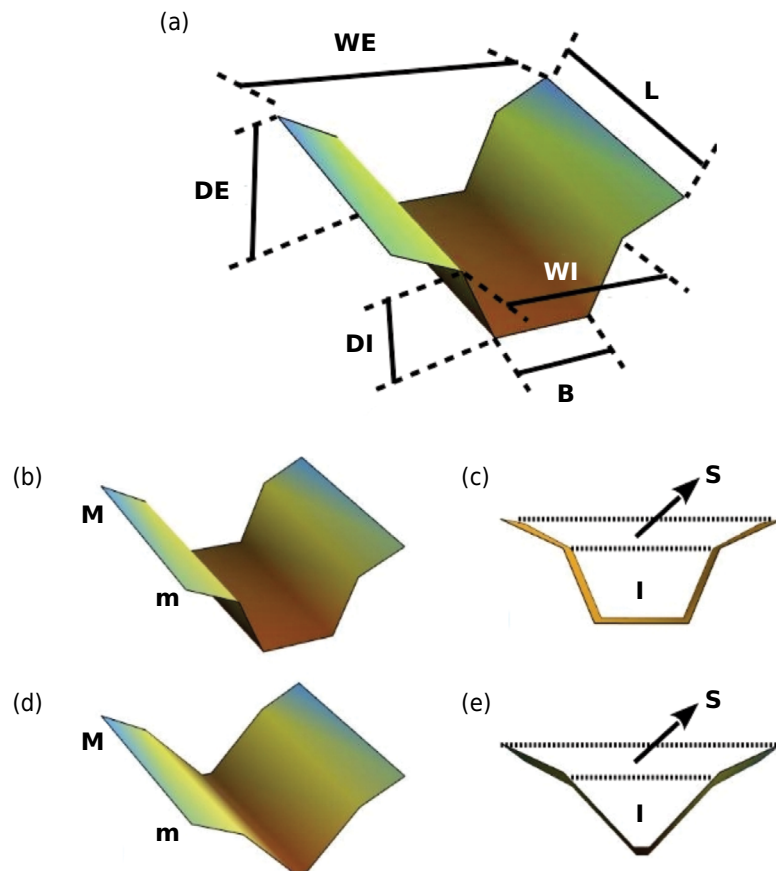


**Figure 4.** Representation of the section formed by two measured points of a linear erosion feature (LEF). (a) overview - WE (width of extreme points of the LEFs), WI (width inside the LEF), DE (depth from WE), DI (depth from WI), L (distance between two measured points) and B (base); (b) and (c) show the perspective and frontal views of a U-shaped linear incision; (d) and (e) show the perspective and frontal views of a Vshaped linear incision. The points M and m represent the two points extremities from which the areas were taken. The letters S and I indicate the frontal view of the upper and lower trapezia, respectively.

(2007). Nash-Sutcliffe Efficiency indicates how well the plot of observed relative frequencies of “WE, WI, DE, and DI” versus simulated probability of occurrences of these variables fits the 1:1 line

$$NSE = 1 - \left[ \frac{\sum_{i=1}^n (Y_i^{obs} - Y_i^{sim})^2}{\sum_{i=1}^n (Y_i^{obs} - Y_i^{mean})^2} \right] \quad \text{Eq. 2}$$

in which  $Y_i^{obs}$  is the  $i$ th observed relative frequencies of “WE, WI, DE, and DI”;  $Y_i^{sim}$  is the  $i$ th probability of “WE, WI, DE, and DI” occurrences simulated by Monte Carlo;  $Y^{mean}$  is the mean of observed relative frequencies, and  $n$  is the total ranges number used in the Monte Carlo simulations. The NSE can assume values between  $-\infty$  and 1, with  $NSE = 1$  being the optimal value. Values between 0 and 1 are generally viewed as acceptable levels of simulation performance, whereas values  $<0$  indicates that the mean observed value is a better predictor than the simulated value (Moriasi et al., 2007).

## RESULTS

The most noticeable aspects of land degradation in the studied area are the marks left on the soil by the intense linear erosion, which moves large portions of sediments from the slopes to the fluvial channel, and damages the seasonal dynamics of the Salitre River. Figure 5 shows the low density of vegetable cover and the large patches of exposed soil in the analyzed area, which allow clear visualization of the linear erosion features (LEFs). The presence of various LEFs can be observed, and the depth of the channels is estimated.

The map shown in figure 6 presents the result of the digitization of the LEFs. From a subtle analysis of the map, 734 LEFs in a complex system of ramifications were observed. The length of such linear erosion ranges from 14 m (for sub-lines on the high slopes) to 1,788 m (for main lines), resulting in a mean length of 199 m. It was also observed that only 3 % of the gullies/rills exceeded 800 m, 25 % were between 200 and 799 m, and 71 % were small, with the extension lower than 200 m. The

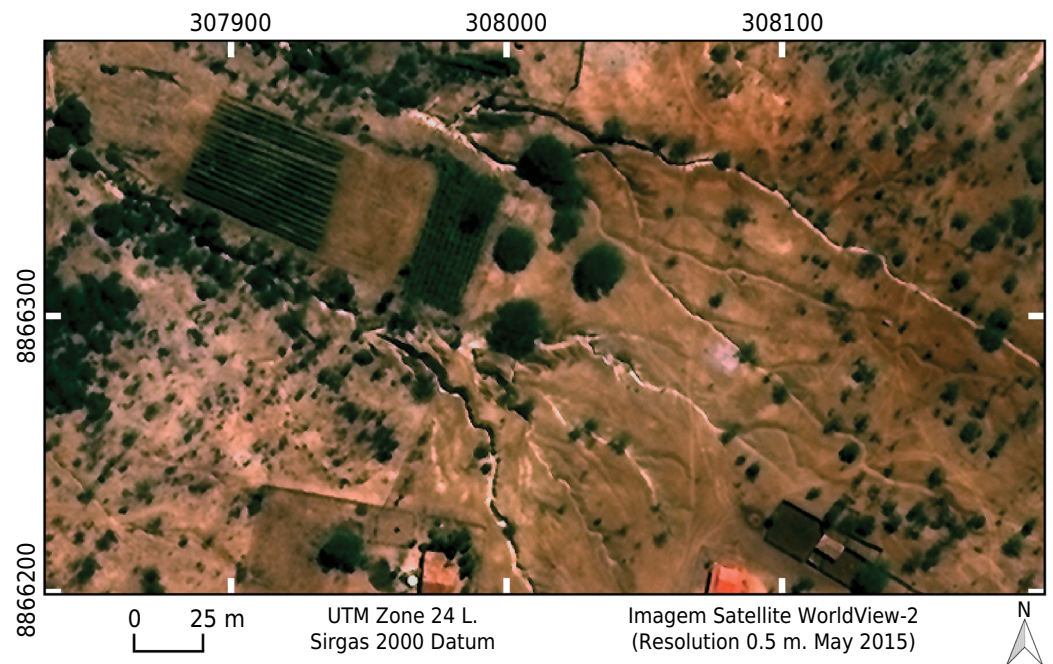


**Figure 5.** Visualization of gullies and larger rills in the surroundings of the community of Taboa – Campo Formoso-BA, Brazil, on a WorldView-2 image. Central point of the image is located at the UTM Coordinate 308066E 8866300N Zone 24L.



sum of the LEFs in the mapped area totaled 145.53 km of visible gullies and rills, over an area of 20.78 km<sup>2</sup> (2,078 ha). Besides, 275 points of connection (confluence) between the LEFs and the fluvial environments in the area were accounted for. Thus, there are 275 systems of erosion channels (most of which are individual channels and do not have associated sub-channels) depositing sediments in the Salitre River and ephemeral tributaries.

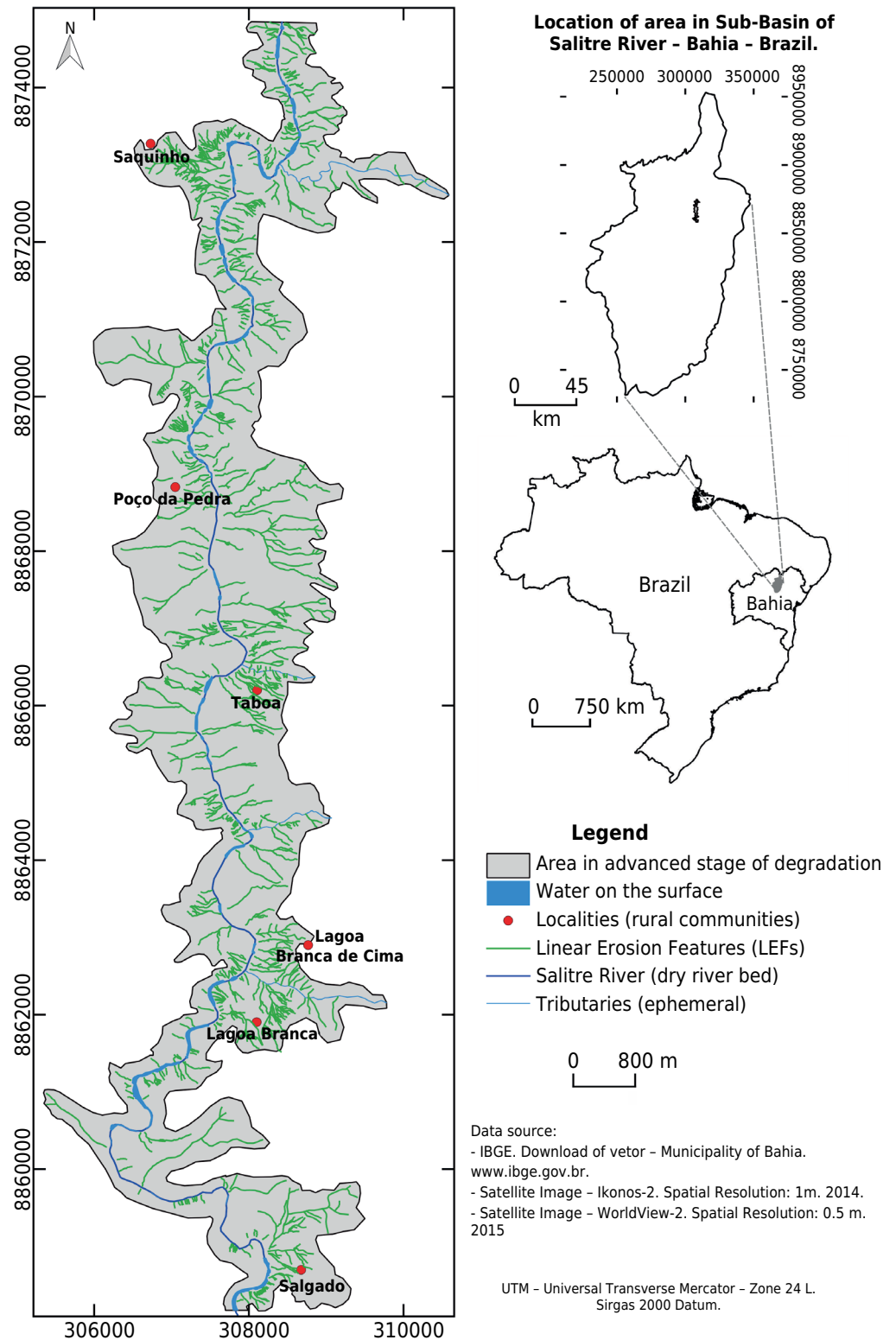


**Figure 6.** Map of Linear Erosive Features (LEFs) located in the middle course of the Salitre River.

The vertical perspective (depth) and the width of the LEFs obtained from the satellite images encourage us to obtain numerical data on the width and depth of a percentage of the erosion features. Therefore, measurements were performed at the field to determine the width, shape, and depth for a total of 11 lines, accounting for a length of 4,117 m, which represented 1.50 % (amount of lines) and 2.83 % (length) of the total found in the interpretation of the satellite images. Although small in percentage, this sampling portion is a significant representation of the condition of the entire area when the pedological, climatic, geological, topographic, phytogeographic, and land use conditions are similar in the entire area.

Thus, each of the WE (width of extreme points of the LEFs), WI (width inside the LEFs), DE (depth from WE), and DI (depth from WI) variables were grouped into 13 classes, according to the probabilities of occurrence. For all observed variables, the Monte Carlo simulation fit the measured data well, as judged visually in figure 7 and by the calculated NSE values, which are: NSE = 0.9 for WE; NSE = 0.7 for WI; NSE = 0.8 for DE, and NSE = 0.6 for DI. The predominance of low values for all variables yields an asymmetric distribution with non-normal behavior, as evidenced by the analysis of figure 7, which shows the data obtained through field study and simulated by Monte Carlo. Based on measured data the non-normality of the hypothesis is confirmed by the Kolmogorov-Smirnov test with 95 % confidence, and it is not possible to use the averaged values to estimate the volume of soil loss due to linear erosion.

In figure 7a (width of extreme points of the LEFs - WE), the class with the highest observed relative frequencies and highest probability of occurrence simulated by Monte Carlo is

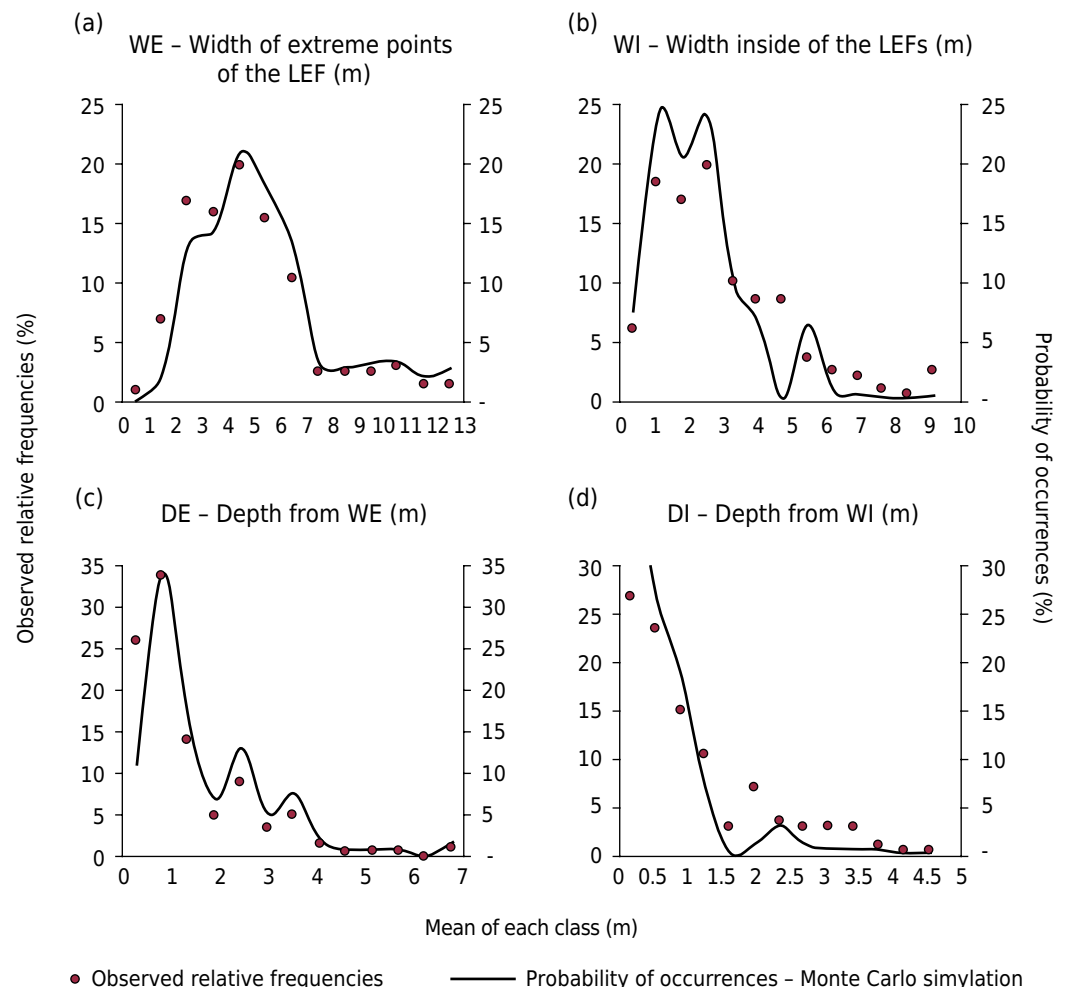


**Figure 7.** Comparison of observed relative frequencies and simulation results of the probability of occurrences by Monte Carlo.

the one with the mean value of 4.5 m. It was also noticed that in both - observed and simulated WE values - more than half of the values were within the range of 2.5 to 5.5 m. Therefore, these classes had the most influential WE range in the Monte Carlo simulations.

In the case of WI, the class with the highest probability of occurrence is the one with an average value of 2.6 m. The figure 7b indicates that more than half of the analyzed LEFs have WI ranging from 0.4 to 2.6 m, and these were the most important values in the Monte Carlo simulation. The mean ( $m$ ), standard deviation ( $\pm m$ ), and coefficient of variation (%) of the measured and simulated WI data were respectively:  $2.96 \pm 1.92$  m, 64.48 %; and  $2.63 \pm 1.33$  m; 50.57 %.

For the DE variable, the class with the highest probability of occurrence is the one with the mean value of 0.8 m. Figure 7c indicates that more than 60 % of the measured and simulated LEFs have WI ranging from 0.3 to 1.4 m. The measured DE data showed an overall mean of  $1.36 \pm 1.20$  m, and coefficient of variation of 88.34 %, while the simulated data showed an overall mean of  $1.97 \pm 1.31$  m and coefficient of variation of 66.82 %.

For the DI variable, the class with the highest probability of occurrence is the one with the mean value of 0.2 m. The measured data showed an overall mean of  $1.07 \pm 0.96$  m and a coefficient of variation of 89.66 %, while the respective statistical indicators for the simulated data were:  $0.8 \pm 0.55$  m; 70 %. According to the data in figure 7d, 70 % of the studied erosion incisions have DI ranging from 0.2 to 0.9 m.

During the measurement of the cross-sections, the shapes of the gullies and rills were also observed, and there were 51.7 % of measured U-shaped gullies and hills with steep walls (which were more or less vertical) and a flat bottom. However, at other points, the same incision was V-shaped (48.3 %), open at the top and narrow at the bottom, indicating that the materials of the subsoil or deeper horizons are more resistant in comparison to the surface horizon. According to the Monte Carlo simulation results, there were 50.4 % of U-shaped gullies and hills. In summary, based on the small difference in percentage, it can be understood that almost half of the linear features along the slopes are V-shaped, while the other half are U-shaped.

It should be considered that the observed incisions extend up to the slope, with tiny widths; therefore, they were not visualized in the images and were not mapped in the present study. Also, there is a significant number of rills spread over the area, connected to gullies and directly linked to fluvial courses or in small independent incisions along the slopes. Due to the limits of the spatial resolution of the satellite images, these rills were not considered in this study.

From the Monte Carlo simulations were then performed based on the data presented in figure 7, and on the shapes of the LEFs. To calculate the soil volume displaced from the slopes, we have applied equation one from using the data obtained in the Monte Carlo simulations. Aiming to compare the results obtained from Monte Carlo simulations with the data collected in field activities, we have performed Monte Carlo simulations for determining the geometrical predictions for 201 cross-sections. From simulations, we obtained that approximately  $11,500 \text{ m}^3$  had been deposited along the Salitre river bed due to the LEFs. The calculation of the soil volume displaced from the slopes to the river obtained from the field activity data is approximately  $12,300 \text{ m}^3$ . Therefore, the agreement between the Monte Carlo simulations and field measurements was approximately 93 %. This finding motivated us to analyze and extrapolate the Monte Carlo simulation to study the volume of soil displaced from the slopes along the entire mapped area. The simulated results allow us to estimate that a total of approximately  $515,000 \text{ m}^3$  of soil had been displaced, by linear erosion, from the slopes along the Southern portion of the middle Salitre River. Since the extension of the Salitre River in this section is 23,900 m, we can conclude that approximately  $22 \text{ m}^3$  of soil was deposited in each linear meter along the river bed and its flood plain.

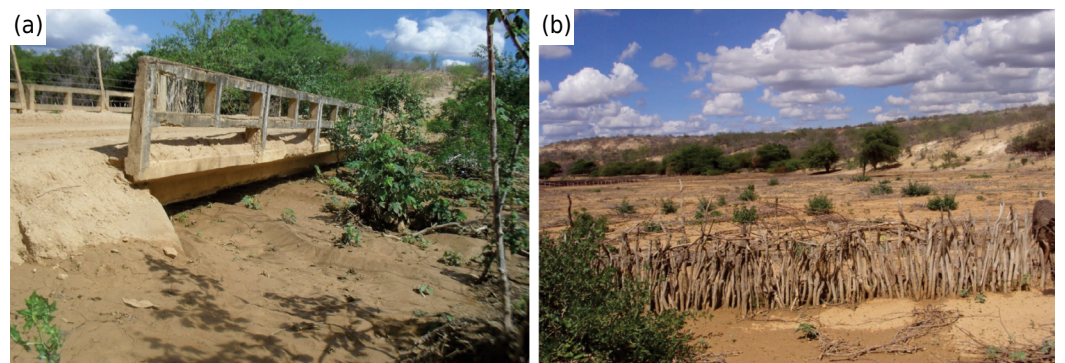
One of the most immediate consequences of the intense erosion processes on the slopes is the accumulation of sediments along the drainage line of the Salitre River. The map in figure 6 also presents the spatial intermittency of surface water along the Salitre River during the period of the highest rainfall in the region (May 2015). The blue marks represent small stationary water bodies, which is not consistent with a fluvial behavior even for intermittent rivers of the semiarid region.

Figure 8 shows a bridge over the studied River, where it can be observed that there is a considerable accumulation of sediment in its bed, evidenced by the filling of the space that existed between the base of the bridge and the river bed. In this process, it is important to consider that the natural conditions of prolonged drought periods and long intermittence of the Salitre River do not provide enough water volume in the riverbed to transport a part of the sediments that arrive through the fluvial channel, thus contributing to the accumulation (siltation).

## DISCUSSION

Several studies have proved the efficiency of the high-resolution satellite image used in the detection of linear erosion features (LEFs). For instance, Shruthi et al. (2011) mapped gullies using Ikonos and GeoEye-1 images in Morocco, highlighting the importance of work as a basis for land use planning and data collection on sediment production. Desprats et al. (2013) used QuickBird images with 0.6 m of spatial resolution to map the erosive phenomenon in the North of Tunisia. Nevertheless, in these works, the efficiency of this technique is verified only in the measurement of length and direction of the LEFs, in such a way that the width and depth of LEFs are not well determined. To avoid such kind of indetermination, in this work, we have used images from WorldView-2, with a resolution of 0.5 m.

Moreover, field activities allowed us to obtain pieces of information on the width and depth of the incisive erosions, and the statistical analysis showed the occurrence probability of the measured widths and depths along the mapped LEFs. Finally, Monte Carlo simulations, a method that has been already used to study erosive process (Nicholls and Stephenson, 1995), was able to simulate these variables from extrapolating the data obtained in field activities to all area, assuming that the soil properties have small variation along the studied area. All these data were joined to estimate, with reasonable confidence, the soil volume that was removed from the slopes, by linear erosion. It is important to highlight that the used methodological procedures can be replicated in other semiarid regions, with low vegetation cover and high soil exposure, aiming to specialize in the LEFs and estimate the soil removed from the slopes.



**Figure 8.** Sediment accumulation along the drainage line of the Salitre River (dry bed). The sediment accumulation reduced the depth of the riverbed, causing the bottom of the channel to come close to the base of the bridge (UTM - Zone-24L 307920E 8862549N) (a). Photograph of the area beside the bridge (b).

The quantity and dimensions of LEF's in the study area showed that the area is under an intense morphodynamics instability, represented by the large amount of soil that is being removed from the slopes and deposited in the Salitre River bed (area with declivity greater than 8 %). Even though a discussion on the causes of the erosive process is out of the scope of this work, the analysis of the map presented in figure 6 evidences that most of the observed area under erosion is located around the village/community of Salgadoinho, Taboa, Lagoa Branca de Cima, and Lagoa Branca. These areas present share the characteristic to have excessive soil use in agriculture activities, pointing to the anthropic contribution in the trigger and acceleration of the linear erosive phenomenon. Nevertheless, LEFs were not observed in the plane areas (with declivity lower than 3 %), even with an accentuated soil use. In this context, environmental conditions (relief and soil) has a crucial influence on the instability of the soil and in the trigger of the erosive process.

The sediment carried to the Salitre River changes the form of the fluvial channel, increasing its width and raising the topographic level of the valley floor (local base level). Such topography changes in the bottom of the riverbed have a direct impact on the dynamics and functioning of the Salitre River, reducing the number of days of the fluvial flow of its waters. It should be noticed that there is a close relationship between the groundwaters and the availability of water on the riverbed (Karmann, 2000). Therefore, the massive accumulation of sediments causes the groundwater level to be at a greater depth concerning the bottom of the fluvial channel. This difference in the water level compromises the maintenance of water on the riverbed, even during rainy periods.

In most dry sections on the riverbed, there is a significant accumulation of sediments, which is a result of the excessive erosion on the slopes. Since most of the 275 points of connection (confluence) between the LEFs and the bed of the Salitre River are found in the dry sections, it can be inferred that the rills and gullies contribute to the increment of sediments at these points. The remobilization of sediment is so intense that river channels cannot carry them, causing extensive filling in the saltpeter river. It is noteworthy that for more than a decade, the Salitre River has not presented water flow in its bed.

Although the causes of this water intermittence along the Salitre River are related to a series of environmental factors, as interventions along the river, constructions, extinction of river sources, and reduction of the water table (Santos, 2016), intense silting must be pointed out as one of them. This silting deposition process results from the erosion processes on nearby slopes (potentially due to the association between human and natural causes) that coincide with the limits of the area presented in this study.

The numbers, dimensions, and spatial density of the linear erosive systems (rills and gullies) identified along the middle course of the Salitre River call attention due to the possibility to form a desertification hotspot. Global warming associated with the extension of grazed and cropped areas should put more regions at high risk of gully erosion (Valentin et al., 2005), which is an important indicator of desertification (Avni, 2005; Zweig et al., 2018). In discussions on the theme of desertification, soil erosion always appears as one of the most critical indicators (Symeonakis et al., 2014; Sarparast et al., 2018). Indeed, it is considered the most severe problem of land degradation and one of the main conditions of desertification in the Brazilian semiarid (Sampaio et al., 2005; Sá et al., 2010). The intense erosion of soils in semiarid environments can point to the existence of an advanced stage of desertification, in which erosion reduces the soil fertility and biological potential of the area and undermines the river channels and water quality. These changes in the natural environment potentiate economic losses with social impacts. In this context, this work contributes to deepening studies on the process of desertification in the Salitre basin, by providing information on the dimensions of the ongoing erosion process and the possible consequences on the dynamics of the Salitre river.

Finally, it is fundamental to consider that the pedological and climatic conditions in the studied area are very different from those in the rest of Brazil. In the middle course of Salitre River, the soils are shallow and poorly developed, and the rainfall is around 400 mm; despite that, the area has a high density of active gullies, certainly above the patterns observed in the semiarid region of Brazilian Northeast.

From using integrated geoenvironmental analysis and evaluation by biophysical and socioeconomic indicators, Santos (2016) stated that the Salitre middle course is an area affected by desertification hotspot. Kulik et al. (2013) point out that these hotspots are places with advanced levels of land degradation. At the same time, Singh and Ajai (2019) argue that these hotspots are extremely vulnerable to degradation/desertification, requiring urgent interventions aiming at their rehabilitation. Therefore, this research pointed out that the Salitre middle course presents landscapes in an advanced stage of soil degradation by linear erosion, reinforcing the significant risk of desertification, demanding an urgent construction of recovery plans for essential ecosystem services in the area.

It is worth highlighting that the desertification is a multivariate phenomenon, and its study must include other indicators. However, the data obtained allow us to state that this area is a possible desertification hotspot, and it is essential to analyze other variables to confirm our statement, in addition to monitoring the increase (over the years) in the number and dimensions of the LEFs.



## CONCLUSIONS




The use of high-resolution satellite images allowed us to point out the spatial distribution and significant density of Linear Erosive Features in an area in the Salitre Sub-basin, located in Bahia, Brazil. Based on the integration of remote sensing and Monte Carlo simulation, we have estimated the volume of soil removed from the slopes by the linear erosive process. The estimate of soil loss on the slopes serves to measure the impact of the linear erosive process acting on the slopes, as well as to detect the significant impacts on the Salitre river clogging and local water dynamics. The information provided confirms that the studied area is under advanced stage of land degradation, and constitutes an element capable of contributing, as an important indicator, in recognition of an ongoing desertification process.




## ACKNOWLEDGMENTS



The authors would like to thank the Federal Institute of Bahia (IF Baiano). We also thank the Bahia Research Support Foundation (FAPESB) and the Secretariat for the Environment of the State of Bahia. V.L.C.S. and A.J.P.S. would like to thank the Brazilian agency CNPq for the financial support. M.L.R. would like to thank IGC/UFMG (Postgraduate Program in Geography).


## AUTHOR CONTRIBUTIONS



**Conceptualization:**  Márcio Lima Rios (equal) and  Alisson Jadavi Pereira da Silva (equal).

**Methodology:**  Márcio Lima Rios (equal),  Alisson Jadavi Pereira da Silva (equal), and  Vagson Luiz Carvalho-Santos (equal).

**Formal analysis:**  Márcio Lima Rios (equal),  Alisson Jadavi Pereira da Silva (equal), and  Vagson Luiz Carvalho-Santos (equal).

**Writing:**  Márcio Lima Rios (equal),  Alisson Jadavi Pereira da Silva (equal), and  Vagson Luiz Carvalho-Santos (equal).

**Supervision:**  Vagson Luiz Carvalho-Santos (equal).

**Project administration:**  Márcio Lima Rios (equal) and  Alisson Jadavi Pereira da Silva (equal).

**Funding acquisition:**  Alisson Jadavi Pereira da Silva (lead).

## REFERENCES

- Avni Y. Gully incision as a key factor in desertification in an arid environment, the Negev highlands, Israel. *Catena*. 2005;63:185-220. <https://doi.org/10.1016/j.catena.2005.06.004>
- Bates DC. Environmental refugees? Classifying human migrations caused by environmental change. *Popul Environ*. 2002;23:465-77. <https://doi.org/10.1023/A:1015186001919>
- Becerril-Piña R, Mastachi-Loza CA, González-Sosa E, Díaz-Delgado C, Bâ KM. Assessing desertification risk in the semi-arid highlands of central Mexico. *J Arid Environ*. 2015;120:4-13. <https://doi.org/10.1016/j.jaridenv.2015.04.006>
- Bigarella JJ. Estrutura e origem das paisagens tropicais e subtropicais. Florianópolis: Editora da UFSC; 2003.
- Borges SVF, Balsamo F, Vieira MM, Iacumin P, Srivastava NK, Storti F, Bezerra FHR. Pedogenic calcretes within fracture systems and beddings in Neoproterozoic limestones of the Irecê Basin, northeastern Brazil. *Sediment Geol*. 2016;341:119-33. <https://doi.org/10.1016/j.sedgeo.2016.05.012>
- Brito Neves BB, Santos RA, Campanha GAC. A discordância angular e erosiva entre os grupos Chapada Diamantina e Bambuí (Una) na folha Mirangaba-Bahia. *Geol USP Ser Cient*. 2012;12:99-114. <https://doi.org/10.5327/Z1519-874X2012000200007>
- Capozzi F, Di Palma A, De Paola F, Giugni M, Iavazzo P, Topa ME, Adamo P, Giordano S. Assessing desertification in sub-Saharan peri-urban areas: case study applications in Burkina Faso and Senegal. *J Geochem Explor*. 2018;190:281-91. <https://doi.org/10.1016/j.gexplo.2018.03.012>
- Carlini BS. Uso de sensoriamento remoto e reconhecimento pedológico para identificação de ambientes na sub-bacia do rio Pacuí, submédio São Francisco [dissertação]. Viçosa, MG: Universidade Federal de Viçosa; 2013.
- Casalí J, Giménez R, Campo-Bescós MA. Gully geometry: what are we measuring? *Soil*. 2015;1:509-13. <https://doi.org/10.5194/soil-1-509-2015>
- Chaplot V, Le Brozec EC, Silvera N, Valentin C. Spatial and temporal assessment of linear erosion in catchments under sloping lands of northern Laos. *Catena*. 2005;63:167-84. <https://doi.org/10.1016/j.catena.2005.06.003>
- Cuomo S, Sala MD, Pierri M. Experimental evidences and numerical modelling of runoff and soil erosion in flume tests. *Catena*. 2016;147:61-70. <https://doi.org/10.1016/j.catena.2016.06.044>
- D'Odorico P, Bhattachan A, Davis KF, Ravi S, Runyan CW. Global desertification: drivers and feedbacks. *Adv Water Resour*. 2013;51:326-44. <https://doi.org/10.1016/j.advwatres.2012.01.013>
- Dai Q, Peng X, Yang Z, Zhao L. Runoff and erosion processes on bare slopes in the karst rocky desertification area. *Catena*. 2017;152:218-26. <https://doi.org/10.1016/j.catena.2017.01.013>
- Dawelbait MAA, Morari F. LANDSAT, spectral mixture analysis and change vector analysis to monitor land cover degradation in a Savanna region in Sudan (1987-1999-2008). *Intl J Water Resources Arid Environ*. 2011;1:366-77.
- Descroix L, Barrios JG, Viramontes D, Poulenard J, Anaya E, Esteves M, Estrada J. Gully and sheet erosion on subtropical mountain slopes: Their respective roles and the scale effect. *Catena*. 2008;72:325-39. <https://doi.org/10.1016/j.catena.2007.07.003>
- Desprats JF, Raclot D, Rousseau M, Cerdan O, Garcin M, Le Bissonnais Y, Ben Slimane A, Fouche J, Monfort-Climont D. Mapping linear erosion features using high and very high-resolution satellite imagery. *Land Degrad Dev*. 2013;24:22-32. <https://doi.org/10.1002/ldr.1094>

- Diamond J. *Collapse: how societies choose to fail or survive*. New York: Penguin; 2005.
- Empresa Brasileira de Pesquisa Agropecuária - Embrapa. Registro de observações meteorológicas - Dados históricos da Estação Salitre. Petrolina: Embrapa Semiárido; 2019 [cited 2019 Dec 20]. Available from: <http://www.cpsa.embrapa.br:8080/index.php?op=dadosmet>
- Gimenez R, Planchon O, Silvera N, Govers G. Longitudinal velocity patterns and bed morphology interaction in a rill. *Earth Surf Proc Land*. 2004;29:105-14. <https://doi.org/10.1002/esp.1021>
- Governo do Estado da Bahia. Plano de recursos hídricos e proposta de enquadramento dos corpos de água da bacia hidrográfica do Rio Salitre: Síntese executiva do PRHS/PF-03. Salvador: Comitê da Bacia Hidrográfica do Rio Salitre; 2017 [cited 2019 Dec 20]. Available from: <http://www.inema.ba.gov.br/wp-content/uploads/2018/06/1149.00-PF-03-R01.pdf>
- Huang S, Siegert F. Land cover classification optimized to detect areas at risk of desertification in North China based on Spot Vegetation imagery. *J Arid Environ*. 2006;67:308-27. <https://doi.org/10.1016/j.jaridenv.2006.02.016>
- Johnson MS, Meskhidze N, Kiliyanpilakkil VP, Gasso S. Understanding the transport of Patagonian dust and its influence on marine biological activity in the South Atlantic Ocean. *Atmos Chem Phys*. 2011;11:2487-502. <https://doi.org/10.5194/acp-11-2487-2011>
- Karamesouti M, Panagos P, Kosmas C. Model-based spatio-temporal analysis of land desertification risk in Greece. *Catena*. 2018;167:266-75. <https://doi.org/10.1016/j.catena.2018.04.042>
- Karmann I. Ciclo da água, água subterrânea e sua ação geológica. In: Teixeira W, Toledo MCM, Fairchild TR, Taioli F, editores. *Decifrando a Terra*. São Paulo: Oficina de Textos; 2000. p. 113-38.
- Krause AK, Franks SW, Kalma JD, Loughran RJ, Rowan JS. Multi parameter fingerprinting of sediment deposition in a small gullied catchment in SE Australia. *Catena*. 2003;53:327-48. [https://doi.org/10.1016/S0341-8162\(03\)00085-7](https://doi.org/10.1016/S0341-8162(03)00085-7)
- Kulik KN, Rulev AS, Yuferev VG. Geoinformation analysis of desertification hotspots in Astrakhan Oblast. *Arid Ecosyst*. 2013;3:184-90. <https://doi.org/10.1134/S2079096113030074>
- Lal M, Mishra SK, Pandey A. Physical verification of the effect of land features and antecedent moisture on runoff curve number. *Catena*. 2015;133:318-27. <https://doi.org/10.1016/j.catena.2015.06.001>
- Landau DP, Binder K. *A guide to Monte Carlo simulations in statistical physics*. 4th ed. Cambridge: Cambridge University Press; 2014.
- Lu X, Wrathall DJ, Sundsøy PR, Nadiruzzaman M, Wetter E, Iqbal A, Qureshi T, Tatem A, Canright G, Engø-Monsen K, Bengtsson L. Unveiling hidden migration and mobility patterns in climate stressed regions: a longitudinal study of six million anonymous mobile phone users in Bangladesh. *Global Environ Chang*. 2016;38:1-7. <https://doi.org/10.1016/j.gloenvcha.2016.02.002>
- Middleton N. Rangeland management and climate hazards in drylands: dust storms, desertification and the overgrazing debate. *Nat Hazards*. 2018;92:57-70. <https://doi.org/10.1007/s11069-016-2592-6>
- Middleton N. Desert dust hazards: a global review. *Aeolian Res*. 2017;24:53-63. <https://doi.org/10.1016/j.aeolia.2016.12.001>
- Moriasi DN, Arnold JG, Van Liew MW, Bingner RL, Harmel RD, Veith TL. Model evaluation guidelines for systematic quantification of accuracy in watershed simulations. *ASABE*. 2007;50:885-900. <https://doi.org/10.13031/2013.23153>
- Myers N. Environmental refugees in a globally warmed world. *Bioscience*. 1993;43:752-61. <https://doi.org/10.2307/1312319>.
- Naime UJ, Carvalho Júnior W, Amaral FCS, Cunha TJJ, Silva EF, Oliveira Neto MB, Fernandes LAC. Levantamento de reconhecimento de baixa intensidade dos solos do entorno do Projeto Salitre-Juazeiro/BA. Rio de Janeiro: Embrapa Solos; 2007. (Boletim de Pesquisa e Desenvolvimento, 118).



- Nash JE, Sutcliffe JV. River flow forecasting through conceptual models Part I – A discussion of principles. *J Hydrol.* 1970;10:282-90. [https://doi.org/10.1016/0022-1694\(70\)90255-6](https://doi.org/10.1016/0022-1694(70)90255-6)
- Nicholls JR, Stephenson DJ. Monte Carlo modelling of erosion processes. *Wear.* 1995;186-187:64-77. [https://doi.org/10.1016/0043-1648\(95\)07156-3](https://doi.org/10.1016/0043-1648(95)07156-3)
- Poesen J, Nachtergaele J, Verstraeten G, Valentin C. Gully erosion and environmental change: importance and research needs. *Catena.* 2003;50:91-133. [https://doi.org/10.1016/S0341-8162\(02\)00143-1](https://doi.org/10.1016/S0341-8162(02)00143-1)
- Rubinstein RY, Kroese DP. *Simulation and the Monte Carlo method.* Hoboken: John Wiley & Sons; 2007.
- Sá IB, Cunha TJF, Teixeira ADC, Angelotti F, Drumond MA. Processos de desertificação no semiárido brasileiro. In: Sá IB, Silva PCG, editores. *Semiárido brasileiro: pesquisa, desenvolvimento e inovação.* Petrolina-PE: Embrapa Semiárido. 2010. p. 125-58.
- Salvati L, Zitti M, Perini L. Fifty years on: long-term patterns of land sensitivity to desertification in Italy. *Land Degrad Dev.* 2016;27:97-107. <https://doi.org/10.1002/ldr.2226>
- Salvati L, Mavrakis A, Colantoni A, Mancino G, Ferrara A. Complex Adaptive Systems, soil degradation and land sensitivity to desertification: a multivariate assessment of Italian agro-forest landscape. *Sci Total Environ.* 2015;521:235-45. <https://doi.org/10.1016/j.scitotenv.2015.03.094>
- Sampaio EVSB, Araújo MSB, Sampaio YSB. Impactos ambientais da agricultura no processo de desertificação no Nordeste do Brasil. *Rev Geografia.* 2005;22:90-112.
- Santos JM. *Indicadores de desertificação no semiárido brasileiro: o caso de Campo Formoso-Bahia [tese].* Niterói: Universidade Federal Fluminense; 2016.
- Sarparast M, Ownegh M, Najafinejad A, Sepehr A. An applied statistical method to identify desertification indicators in Northeastern Iran. *Geoenviron Disasters.* 2018;5:3. <https://doi.org/10.1186/s40677-018-0095-3>
- Shruthi RB, Kerle N, Jetten V. Object-based gully feature extraction using high spatial resolution imagery. *Geomorphology.* 2011;134:260-8. <https://doi.org/10.1016/j.geomorph.2011.07.003>
- Sidorchuk A. Stochastic components in the gully erosion modelling. *Catena.* 2005;63:299-317. <https://doi.org/10.1016/j.catena.2005.06.007>
- Silva AB. *Recursos hídricos subterrâneos da bacia do rio Salitre, Bahia: uso sustentável na indústria do Mármore Bege Bahia.* Salvador: CBPM; 2006.
- Singh RB, AJAI. A composite method to identify desertification 'hotspots' and 'brightspots'. *Land Degrad Dev.* 2019;30:1025-39. <https://doi.org/10.1002/ldr.3290>
- Spinoni J, Vogt J, Naumann G, Carrao H, Barbosa P. Towards identifying areas at climatological risk of desertification using the Köppen-Geiger classification and FAO aridity index. *Int J Climatol.* 2015;35:2210-22. <https://doi.org/10.1002/joc.4124>
- Symeonakis E, Karathanasi N, Koukoulas S, Panagopoulos G. Monitoring sensitivity to land degradation and desertification with the environmentally sensitive area index: the case of Lesvos Island. *Land Degrad Dev.* 2014;22:184-97. <https://doi.org/10.1002/ldr.2285>
- United Nations. *United Nations convention to combat desertification in those countries experiencing serious drought and/or desertification, particularly in Africa. Final text of the Convention; 1994 [cited 2019 Jul 08].* Available from: [https://www.unccd.int/sites/default/files/relevant-links/2017-01/English\\_0.pdf](https://www.unccd.int/sites/default/files/relevant-links/2017-01/English_0.pdf).
- United States Geological Survey - USGS. *Shuttle Radar Topography Mission - SRTM elevation data with 30m resolution; 2014 [cited 2018 Mar 18].* Available from: <https://earthexplorer.usgs.gov/>.
- Valentin CJ, Poesen J, Li Y. Gully erosion: impacts, factors and control. *Catena.* 2005;63:132-53. <https://doi.org/10.1016/j.catena.2005.06.001>
- Vieira RDSP, Tomasella J, Alvalá RCS, Sestini MF, Affonso AG, Rodriguez DA, Barbosa AA, Crepani E, Oliveira SBP. Identifying areas susceptible to desertification in the Brazilian northeast. *Solid Earth.* 2015;6:347-60. <https://doi.org/10.5194/se-6-347-2015>

Wasson RJ, Caitcheon G, Murray AS, McCulloch M, Quade J. Sourcing sediment using multiple tracers in the catchment of Lake Argyle, Northwestern Australia. *Environ Manage.* 2002;29:634-46. <https://doi.org/10.1007/s00267-001-0049-4>

Zweig R, Filin S, Avni Y, Sagy A, Mushkin A. Land degradation and gully development in arid environments deduced by mezzo-and micro-scale 3-D quantification- The Negev Highlands as a case study. *J Arid Environ.* 2018;153:52-65. <https://doi.org/10.1016/j.jaridenv.2017.12.006>